PNC-TN9410 87-005

Presented at the 2nd ASME-JSME
Thermal Engineering Joint Conference
Honolulu, Hawai, 22-27 March 1987

Full Scale Dryout Test and Analysis on The Time to Dryout during Flow and Power Transients

Jan, 1 9 8 7

OARAI ENGINEERING CENTER

POWER REACTOR AND NUCLEAR FUEL DEVELOPMENT CORPORATION

Ⓐ

PNC-TN9410 87-005
Jan., 1987

Full Scale Dryout Test and Analysis on The Time to Dryout during Flow and Power Transients

Satoru Sugawara(*) and Kiminori Shiba(*)

Abstract

Transient dryout has been tested on a full scale electric heater mockup of an ATR 36-rod fuel bundle during fast flow and power transients which could take place in loss of flow or overpower accidents. The analyses were also carried out in order to investigate the prediction capability of the onset of transient dryout. The time to dryout and the dryout power during transient could be well and/or conservatively predicted based on the local steam quality, local mass flux, local heat flux and steady state CHF correlation. Furthermore, transient effect on dryout could be well traced by FIDAS code based on the transient three-fluid nine-equation model and the film dryout criterion.

(*) Heat Transfer Section, Safety Engineering Division, OEC, PNC

CONTENTS

1. INTRODUCTION

The prediction of the onset of dryout during transient is one of the important problems in the safety analysis of nuclear reactors which includes flow transient due to pump failure, overpower transient as caused by control rod withdrawal, loss of coolant accident (LOCA) due to a primary pipe break and anticipated transients without scram (ATWS).

In this regard, Mayinger[1] and Leund[2] reviewed a lot of investigations on the transient dryout experiments[3]~[9], and pointed out that the onset of dryout during transients can be predicted using the steady state CHF correlation and local parameters calculated by the computer codes. However, there are few experiments which were carried out using a full scale mock up of a fuel bundle, and these transient experiment were carriedout under comparatively slow transient conditions. Moreover, although a lot of researchers have reported that the transient dryout power or CHF is larger than that of the steady state condition in fast transients, this transient effect has not been so far confirmed analytically.

Thus, the purposes of this study are to verify from full scale experiments that the onset of transient dryout can be precisely and conservatively predicted by using the steady state CHF correlation in a wide variety of flow and power transient conditions, and to explain the transient effect on dryout phenomenologically by the three-fluid modeling and the film dryout criterion.

2. EXPERIMENT

2.1 Apparatus

Experiments were carried out using the 14 MW Heat Transfer Loop (HTL) heated by electric power. As shown in Fig. 1, HTL consists of a test section housing a heater rod bundle, an electric power supply system connected with the bundle, a steam drum, a high pressure condenser, a subcooler, a pressurizer, circulating pumps, etc. The maximum operating condition of HTL is 10 MPa of pressure, 590 K of temperature, and 8×10^4 kg/h of flow rate.

The heater rod bundle in the test section is a full scale mock up of

a fuel bundle designed for the 600 MWe demonstration plant of ATR, and has a heated length of 3.7 m, heat transfer area of 6.06 m^2, flow area of 4,788 mm^2 and hydraulic equivalent diameter of 9.3 mm. In the heater rod bundle, 36 heater rods are arrayed in three concentric circular layers surrounding a non-heated center rod. The rods are made of stainless steel (SUS316), and their surface is polished up about 1 μm of roughness. Power shape of the heater bundle is axially uniform and laterally non-uniform such as 1.20/0.84/0.72 from the outermost to inner layer. Although all heater rods have the same diameter of 14.5 mm, the rod thickness between one and another layer is different so as to simulate radial power distribution across the fuel bundle. The thickness are 1.32, 0.90 and 0.76 mm from the outermost to inner layer. These heater rods are positioned in the bundle with ring type spacers which are equivalent in shape with those to be used in the fuel bundles of ATR.

Surface temperature of heater rods were measured with sheathed chromel-alumel thermocouples of 0.5 mm in outer diameter. As shown in Fig. 2, the thermocouples are welded, immediately upstream of the spacers, on the heater rods in the outermost and middle layers, since previous dryout experiments show that dryout usually occurs on these rods. In addition, several thermocouples are attached axially and azimuthally on the heater rod in order to measure axial and azimuthal wall temperature distribution and dryout spreading.

2.2 Experimental Procedures and Conditions

The following two types of transient experiments were performed.

- flow decay with constant power (132 runs)
  (TRFD; TRansient experiment during Flow Decay)
- power excursion with constant flow (146 runs)
  (TRPE; TRansient experiment during Power Excursion)

The flow transients postulated in reactors were simulated by step- or ramp-wise controlled flow reductions at the inlet of test section. These flow reductions were made by closing the flow control valve set up at one

of the parallel inlet pipe lines, and the flow reduction rate was adjusted by the valve closing time and reduction width. (Fig. 3(a)) During all flow transients the power has been kept constant at about 80% of the equivalent steady state dryout power for the initial flow rate. The power transients were simulated by a ramp-wise increase of the electric power to the heaters starting at an initial power of about 80% of the equivalent steady state dryout power. (Fig. 3(b)) And additional tests were also performed starting at an different initial power level to confirm the effect of that.

The experiments were carried out under the wide range of initial and transient conditions which include actual conditions of ATR as shown in Table 1.

Table 1 Experimental Conditions of The Transient Test

		TRFD (132 runs)	TRPE (146 runs)
pressure	MPa	2-7	2-7
inlet subcooling	K	10-80	10-100
initial flow rate	t/h/bundle	10-50	10-50
initial bundle power	MW	2-6	0.50-5.5
flow reduction rate	$kg/m^2/s^2$	up to 11,000	≃ 0
flow reduction rate	%/s	up to 500	≃ 0
power increase rate	$MW/m^2/s$	≃ 0	up to 0.76
power increase rate	%/s	≃ 0	up to 500

In these experiments, system pressure is defined at the test section exit, and the flow reduction rate is defined at the test section inlet. Flow rate is measured with turbine and drag disk flow meters at the inlet pipe of test section. Electrical power was determined by current and voltage measurements between the upper and lower power connections of the test section. Trip temperature of thermocouples was set at 780 K, and the onset of dryout was defined by initiation of continuous wall temperature rise. To prevent the heater rod bundle from damage, power supply to the

bundle was reduced within 0.1 sec by ~30% from the initial power when surface temperature reached to the trip temperature.

Data were acquired at a rate of 32 frames per second. Measuring accuracy was estimated at ±0.5% for system pressure, ±1% for heating power, ±0.5% for coolant temperature, ±2% for coolant flow rate, ±0.75% for surface temperature.

3. EXPERIMENTAL RESULTS

Figure 4 shows a typical result on the dryout spreading and wall temperature distribution during flow transient. In any case of the present transient experiments, dryout was observed to occur at first in the outermost layer, being localized on the heater rod surface facing subchannels between the outermost and middle layers immeadiately upstream of the spacer designated by No.3 in Fig.2; then the dryout spread axially and azimuthally. The maximum wall temperature rise was observed at the point where dryout was initiated. There is no significant difference in dryout position between the foregoing steady state and present transient experiments, which implies that flow transient gives no influence on spacial characteristics of dryout behavior for a rod bundle with an axially uniform power distribution.

Figure 5 shows a typical flow transient result together with histories of the heater rod surface temperature, inlet flow rate, bundle power, system pressure and inlet/outlet pressure difference. In this case, inlet flow rate decreased from 34 t/h to about a half within 0.3 sec while bundle power was kept constant at 5.2 MW.

Finally, Figure 6 shows a typical power transient result for the case where the power increases at 53%/sec from the initial bundle power of 4.7 MW with the constant value of 32 t/h.

4. ANALYSIS

4.1 CONVENTIONAL ANALYSIS ON THE TIME TO DRYOUT

In order to investigate how accurately the onset of transient dryout can be predicted by a thermal-equilibrium transient analysis coupled with design correlations of steady state CHF, two-phase pressure drop multipliers[10], void fraction[11] and so on, the transient experiments were analysed with the onedimensional multi-node code TRANEX whose calculational scheme is almost the same with the COBRA-IV except the mixing calculation. The correlations involved in the TRANEX code were developed based on full scale mockup tests under actual operating conditions. In particular, the steady state CHF correlation is formulated from data of full scale mock up tests as follows.

$$q_c = (a + bx + cx^2) \prod_i F_i \qquad (1)$$

where a, b, c are constants, x is the steam quality and F_i are correction factors dependent on the system pressure, inlet subcooling, spacer pitch, fuel eccentricity, and local and axial power distributions. The transient experiments were analysed with the help of the following actually measured input data:

- bundle dimensions
- channel inlet flow rate versus time
- channel outlet pressure versus time
- channel inlet temperature versus time
- channel power generation versus time and position.

Analytical results including the time history of test section pressure drop, the time to dryout from the beginning of transient and the critical dryout power were compared with measurements.

Figure 7 shows comparisons of the test section pressure drop histories during both of flow and power transients between measurement and calculation. As shown in this figure, predicted histories agree well with the measurement. This indicates the hydrodynamic calculation of the code is reasonable for

the transient analysis. On the other hand, an accuracy of TRANEX code prediction for the steady state dryout power has been estimated at ±4%, as shown in Fig. 8.

Furthermore, calculated CPR variations are superimposed on experimental results in the upper part of Figs. 5 and 6. This CPR is calculated for the immeadiately upstream of spacer #3 where first dryout occurs. The dryout criterion in the analysis is CPR $\leqq$ 1.0. As shown in Figs. 5 and 6, predicted dryout times agree with experiment in both of flow and power transients. The dryout continues in the period while the value of CPR are kept less than unity, and then rewetts just after when the value of CPR recovers greater than unity.

Comparisons between prediction and measurement on the time to dryout are summarized in Fig. 9 for the flow transient and in Fig. 10 for the power transient. As shown in Fig. 9, the predicted time to dryout during flow transient agrees well with the measurement within ±0.30 second; while, as shown in Fig. 10, the time to dryout during power transient can be well and/or conservatively predicted.

This leads to the conclusion that the dryout during flow and power transients can be predicted precisely or conservatively on the basis of the steady state CHF and local properties.

4.2 TRANSIENT AND STEADY STATE DRYOUT POWER

The critical dryout power during tansients can be evaluated by ECPR (Experimental Critical Power Ratio) defined as follows.

$$\text{ECPR} \equiv \frac{\text{critical power predicted by the steady state CHF correlation}}{\text{measured critical power}} \quad (2)$$

In the present transient experiments, the measured critical power is determined as the power at which first continuous temperature rise occurred on heater rod surface. Accordingly, the ratio of dryout power between the transient and steady state is given by

$$\frac{\text{Transient dryout power}}{\text{Steady state dryout power}} \equiv \frac{1}{\text{ECPR}} \quad \text{at the measured dryout time .} \qquad (3)$$

A typical relation between the inlet flow decrease rate and 1/ECPR is indicated in Fig. 11 under the 7MPa condition. Figure 11 shows that the transient dryout power during the flow transient is almost the same as the steady state dryout power within an error band of steady state data (±4%). This fact implies that change in flow rate at the end of heated section where dryout occurs at first, is diminished due to voiding in a heated channel although inlet flow rate is rapidly reduced.

In contrast with flow transient, the transient effect in the power excursion is clearly recognized from Fig. 12. A measured relation of the power increase rate versus 1/ECPR shows that the transient dryout power becomes larger according to the increase in power increase rate.

4.3 ANALYSIS BY THE THREE-FLUID MODEL

The transient effect on the dryout power during flow and power transients has been phenomenalogically analysed by the FIDAS code developed by author[14]. FIDAS code is a one-dimensional multi-node thermal non-equilibrium and transient thermohydraulic analysis code based on the three-fluid (liquid film, entrained droplet and vapor) model and 'the film dryout criterion' recommended by AERE Harwell researchers[12][13].

Three-fluid model is formulated in term of three sets of conservation equations governing the balance of mass, momentum and energy of each phase as follows.

Continuity Equations

for the steam:

$$\frac{\partial}{\partial t}(\alpha_G \rho_G) + \frac{1}{A}\frac{\partial}{\partial z}(\alpha_G \rho_G u_G A) = -\Gamma_F + \Gamma_E \quad , \qquad (4)$$

for the liquid film:

$$\frac{\partial}{\partial t}(\alpha_F \rho_F) + \frac{1}{A}\frac{\partial}{\partial z}(\alpha_F \rho_F u_F A) = -\Gamma_F + -(m_D \frac{S}{A} m_E) \quad , \tag{5}$$

for the entrained droplet:

$$\frac{\partial}{\partial t}(\alpha_E \rho_E) + \frac{1}{A}\frac{\partial}{\partial z}(\alpha_E \rho_E u_E A) = -\Gamma_E - -(m_D \frac{S}{A} m_E) \quad , \tag{6}$$

and,

$$\alpha_G + \alpha_F + \alpha_E = 1 \quad . \tag{7}$$

Momentum Equations

for the steam:

$$\frac{\partial}{\partial t}(\alpha_G \rho_G u_G) + \frac{\partial}{\partial z}(\alpha_G \rho_G u_G^2) = -\alpha_G \frac{\partial P}{\partial z} - \overline{A_{FG}}\tau_{FG} - \overline{A_{EG}}\tau_{EG}$$

$$- \overline{A_{WG}}\tau_{WG} + (\Gamma_{FG} u_F - \Gamma_{GF} u_G) + (\Gamma_{EG} u_E - \Gamma_{GE} - u_G)$$

$$- \alpha_G \rho_G g \cos\theta \quad , \tag{8}$$

for the liquid film:

$$\frac{\partial}{\partial t}(\alpha_F \rho_F u_F) + \frac{\partial}{\partial z}(\alpha_F \rho_F u_F^2) = -\alpha_F \frac{\partial P}{\partial z} + \overline{A_{FG}}\tau_{FG} - \overline{A_{EF}}\tau_{EF}$$

$$- \overline{A_{WF}}\tau_{WF} - (\Gamma_{FG} u_F - \Gamma_{GF} u_G) + \frac{S}{A}(m_D u_E - m_E u_F)$$

$$- \alpha_F \rho_F g \cos\theta \quad , \tag{9}$$

for the entrained droplet:

$$\frac{\partial}{\partial t}(\alpha_E\rho_E u_E) + \frac{\partial}{\partial z}(\alpha_E\rho_E u_E^2) = -\alpha_E\frac{\partial P}{\partial z} + \overline{A_{EG}}\tau_{EG} + \overline{A_{EF}}\tau_{EF}$$

$$- \overline{A_{WE}}\tau_{WE} - (\Gamma_{EG}u_E - \Gamma_{GE}u_G) - \frac{S}{A}(m_D u_E - m_E u_F)$$

$$- \alpha_E\rho_E g\cos\theta \quad . \tag{10}$$

Energy equations

for the steam:

$$\frac{\partial}{\partial t}(\alpha_G\rho_G H_G) + \frac{1}{A}\frac{\partial}{\partial z}(\alpha_G\rho_G H_G u_G A) = -P\frac{\partial\alpha_G}{\partial t} - \frac{P}{A}\frac{\partial}{\partial z}(\alpha_G u_G A)$$

$$+ \Gamma_{FG}H_{g,sat} - \Gamma_{GF}H_{\ell,sat} + \Gamma_{EG}H_{g,sat} - \Gamma_{GE}H_{\ell,sat} + Q_G \quad ,$$

for the liquid film:

$$\frac{\partial}{\partial t}(\alpha_F\rho_F H_F) + \frac{1}{A}\frac{\partial}{\partial z}(\alpha_F\rho_F H_F u_F A) = -P\frac{\partial\alpha_F}{\partial t} - \frac{P}{A}\frac{\partial}{\partial z}(\alpha_F u_F A)$$

$$- \Gamma_{FG}H_{g,sat} + \Gamma_{GF}H_{\ell,sat} + Q_F + \frac{S}{A}(m_D H_E - m_E H_F) \quad , \tag{12}$$

for the entrained droplet:

$$\frac{\partial}{\partial t}(\alpha_E\rho_E H_E) + \frac{1}{A}\frac{\partial}{\partial z}(\alpha_E\rho_E H_E u_E A) = -P\frac{\partial\alpha_E}{\partial t} - \frac{P}{A}\frac{\partial}{\partial z}(\alpha_E u_E A)$$

$$- \Gamma_{EG}H_{g,sat} + \Gamma_{GE}H_{\ell,sat} + Q_E + \frac{S}{A}(m_D H_E - m_E H_F) \quad . \tag{13}$$

The three-fluid heat transfer model is indicated schematically in Fig. 13 for the pre- and post-dryout regime. Wall and interfacial heat

transfer modes and constitutive correlations for the three-fluid model are summarized in Table 2. The interfacial shear stress between liquid film and steam is given by Wallis[15] correlation, besides, the wall shear stress and drag force of droplet are given by conventional single phase correlations. The average droplet diameter which affects the heat transfer between droplets and steam is determined by the critical Weber number. The entrainment rate of droplets from the liquid film m_E, and the deposition rate of droplets on to the liquid film m_D were used as adjusted ones to the steady state dryout data of the same bundle in advance of the transient analysis. Primary inputs for boundary conditions of the FIDAS code are the same as ones for previously mentioned conventional analysis.

Analytical results on the ratio of dryout power between transients and the steady states are shown in Figs. 11 and 12, compared with the measurements. As shown in Fig. 11, analytical result by FIDAS code agrees with the measurement and indicates that the transient effect is small in the flow transient, although the transient dryout power becomes slightly larger as increase of the inlet flow reduction rate. In addition, for the power transient result, analysis traces well the measured increasement of transient dryout power to the steady state value.

It is demonstrated from these evaluations that analysis by the transient three-fluid modeling coupled with the film dryout criterion gives prediction of the transient effect on dryout, in good agreement with experiments.

5. CONCLUSION

The prediction capabilities of the transient dryout was evaluated based on the full scale dryout test during flow and power transients under conditions which include actual conditions of ATR.

The time to dryout and the dryout power during transients could be well and/or conservatively predicted by TRANEX code based on the thermal-equilibrium mixture model coupled with the steady state CHF correlation.

Furthermore, the transient effect on the dryout observed in present study could be well traced by FIDAS code based on the transient three-fluid model and the film dryout criterion.

6. REFERENCES

1. F. Mayinger, "Accident Behavior - A Review : Problems and Status of Knowledge," European Two-Phase Flow Meeting, Erlangen (June 1976).
2. J.C.M. Leung, "Critical Heat Flux under Transient Conditions : A Literature Survey," NUREG/CR-0056, 1978.
3. S. Aoki, A. Inoue, Y. Kozawa, T. Furubayashi, M. Aritomi, T. Nakajima and H. Okazaki, "Critical Heat Flux Under Transient Condition (Case of Transient Heat Input)," Intl. Mtg. Reactor Heat Transfer, Karlsruhe, Germany, Paper No.2 (Oct. 1973).
4. L.S. Tong, H.E. Bishop, J.E. Casterline and B. Matzner, "Transient DNB Test on CVTR Fuel Assembly," ASME paper No.65-WA/NE-3 (1965).
5. D. Hein and F. Mayinger, "Burnout Power in Transient Conditions," Seminar on Two-Phase Flow Thermohydraulics, Rome (June 1972).
6. L.A. Zielke and R.H. Wilson, "Transient Critical Heat Flux and Spacer Grid Studies," Nucl. Tech., 24, p.13 (1974).
7. R.T. Lahey, B.A. Shiralkar, J.M. Gonzalez, and L.E. Schnebley, "The Analysis of Transient Critical Heat Flux," GEAP-13249 (1972).
8. D. Moxon and P.A. Edwards, "Dryout During Flow and Power Transients," AEEW-R-553 (1967).
9. M. Cumo, F. Fabrizi and G. Parazzi, "Transient Critical Heat Flux in Loss-of-Flow-Accidents (LOFA)," Int. J. Multiphase Flow, 4, p.497, 1978.
10. S. Sugawara and T. Kobori, "Analysis of Coolant Flow Distribution in FUGEN Reactor Core," Proceedings ANS/ASME/NRC Topical Meeting on Nuclear Reactor Thermohydraulics, NUREG/CP-6014, 1980.
11. D.R.H. Beattie and S. Sugawara, "An application of Mixing Length Theory to Two-phase Flow Thermohydraulics in ATR," PNC N941 85-10, 1985.
12. G.F. Hewitt and N.S. Hall-Taylor, "Annular Two-Phase Flow," Pergamon Press, 1970.
13. P.B. Whalley, "The Calculation of Dryout in A Rod Bundle," Int. J. Multiphase Flow, Vol.3, pp.501-515, 1977.
14. S. Sugawara, K. Inukai and K. Shiba, "Development of Transient Dryout Analysis Code FIDAS based on the Three-Fluid Model," PNC Internal Report.
15. G.B. Wallis, "One-Dimensional Two-Phase Flow," McGraw-Hill, pp.318-322, 1969.

7. NOMENCLATURE

A = cross sectional area (m^2)
$\overline{A}$ = surface area per unit volume (1/m)
CHF = critical heat flux (w/m^2)
D = equivalent diameter (m)
F = gray body factor (-)
FF = correction factor for CHF (-)
G = mass flux ($kg/m^2 \cdot s$)
H = specific enthalpy (J/kg)
h = heat transfer coefficient ($W/m^2 \cdot K$)
k = thermal conductivity ($W/m \cdot K$)
m_D = deposition rate of droplets onto the liquid film ($kg/m^2 \cdot s$)
m_E = entrainment rate of droplets from the liquid film ($kg/m^2 \cdot s$)
P = pressure (Pa, MPa)
Pr = Prandtl number (-)
Q = heat transfered per unit volume ($J/m^3 \cdot s$)
Q = bundle power (MW)
q = heat flux (W/m^2)
Re = Reynolds number (-)
S = wetted perimeter (m)
T = temperature (K)
t = time (s)
u = velocity (m/s)
x = steam quality (-)
W = mass flow rate (t/h)

Greek letters

α = volumetric fraction (-)
Γ = evaporated or condensed mass ($kg/m^3 \cdot s$)
δ = droplet diameter (m)
η = evaporation coefficient (-)
μ = viscosity ($kg/m \cdot s$)
ρ = specific weight (kg/m^3)

σ_B = Stefan-Boltzmann constant = 5.67032×10^{-8} (W/m^2K^4)

τ = shear stress (N/m^2)

Subscripts

C = critical

DO = dryout

E = entrainment

F = liquid film

G = steam (gas core)

g = steam

in = inlet

ini = initial

ℓ = liquid

sat = saturated

RAD = radiation

W = heated wall

Table 2 Constitutive Equations used in FIDAS

Convection between wall and liquid film or steam

$$h_{WF} = 0.023 \frac{k_F}{D} Re_F^{0.8} Pr_F^{0.4} \quad \text{(for pre-dryout regime)} \quad , \tag{14}$$

or

$$h_{WG} = 0.023 \frac{k_G}{D} Re_G^{0.8} Pr_G^{0.4} \quad \text{(for post-dryout regime)} \quad . \tag{15}$$

Convection between liquid film and steam

$$h_{FG} = 0.023 \frac{k_G}{D_{FG}} Re_{FG}^{0.8} Pr_G^{0.4} \quad , \tag{16}$$

where

$$Re_{FG} = \frac{\alpha_G \rho_G |u_G - u_F| D_{FG}}{\mu_G} \quad . \tag{17}$$

Convection between droplet and steam

$$h_{GE} = \frac{k_G}{\delta} \left\{ 2 + 0.55 \left[\frac{\rho_G |u_G - u_E| \delta}{\mu_G} \right]^{0.5} pr_G^{0.33} \right\} \quad . \tag{18}$$

Evaporation of droplet on the wall

$$q_{WE} = \eta m_D H_{\ell g} \quad . \tag{19}$$

Radiation from wall to steam and droplet

$$q_{WG,RAD} = F_{WG} \sigma_B (T_W^4 - T_G^4) \quad \text{(to steam)} \quad , \tag{21}$$

and

$$q_{WE,RAD} = F_{WE} \sigma_B (T_W^4 - T_G^4) \quad \text{(to droplet)} \quad . \tag{22}$$

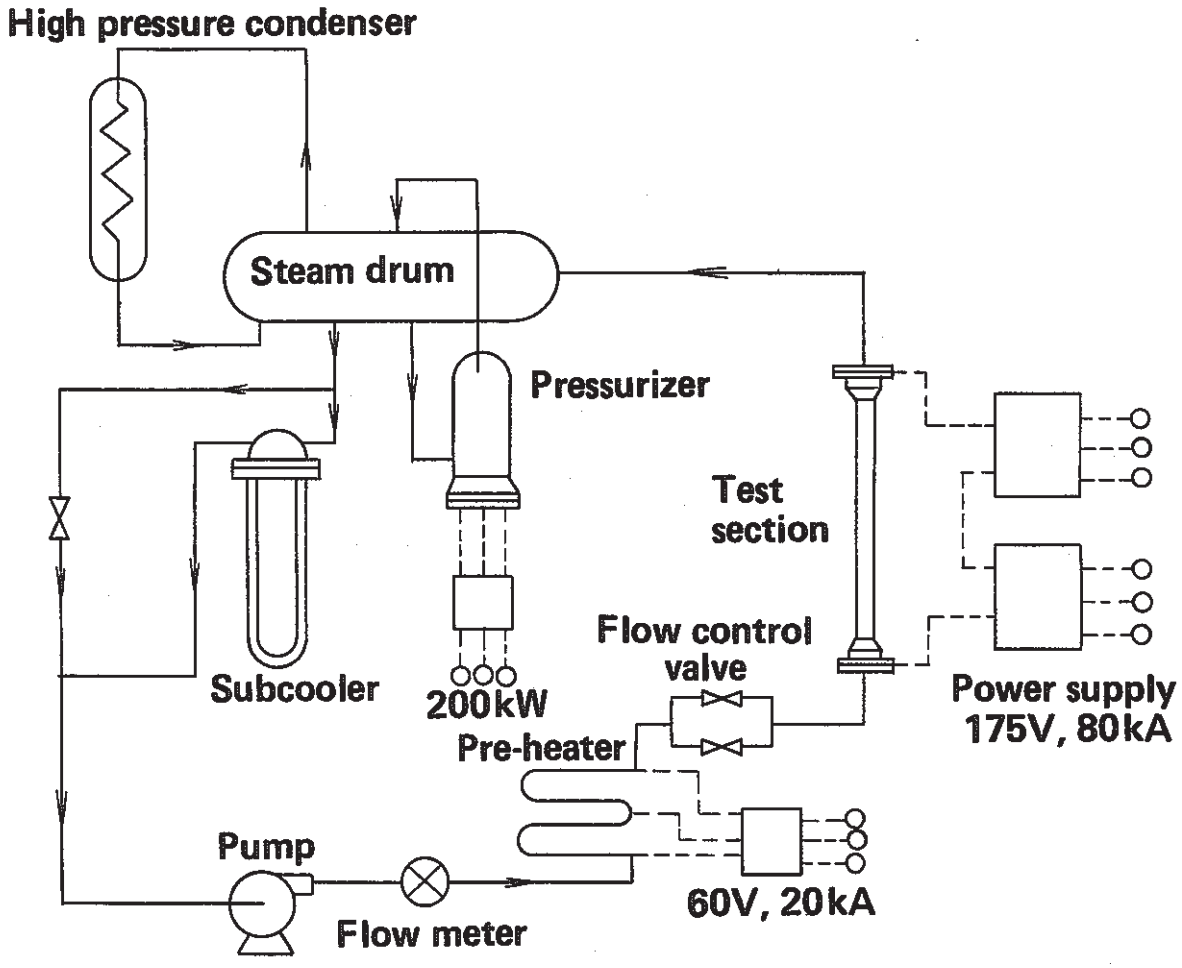

Fig. 1 Flow Diagram of 14MW Heat Transfer Loop (HTL)

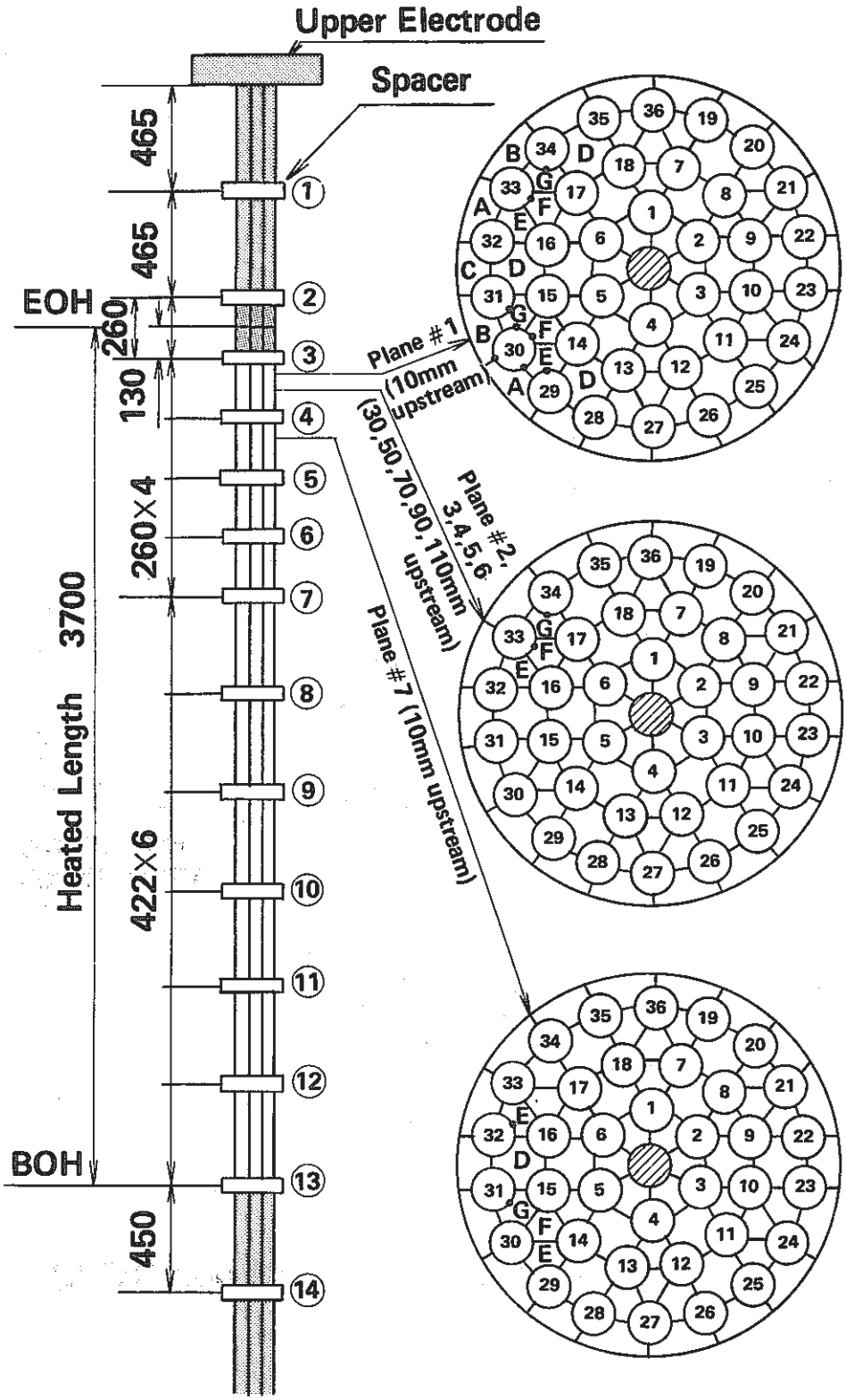

Local Power Distribution : Outer to Inner : 1.20/0.84/0.72

Axial Power Distribution : Uniform

Fig. 2 Fuel Assembly Configuration and Thermocouple Locations

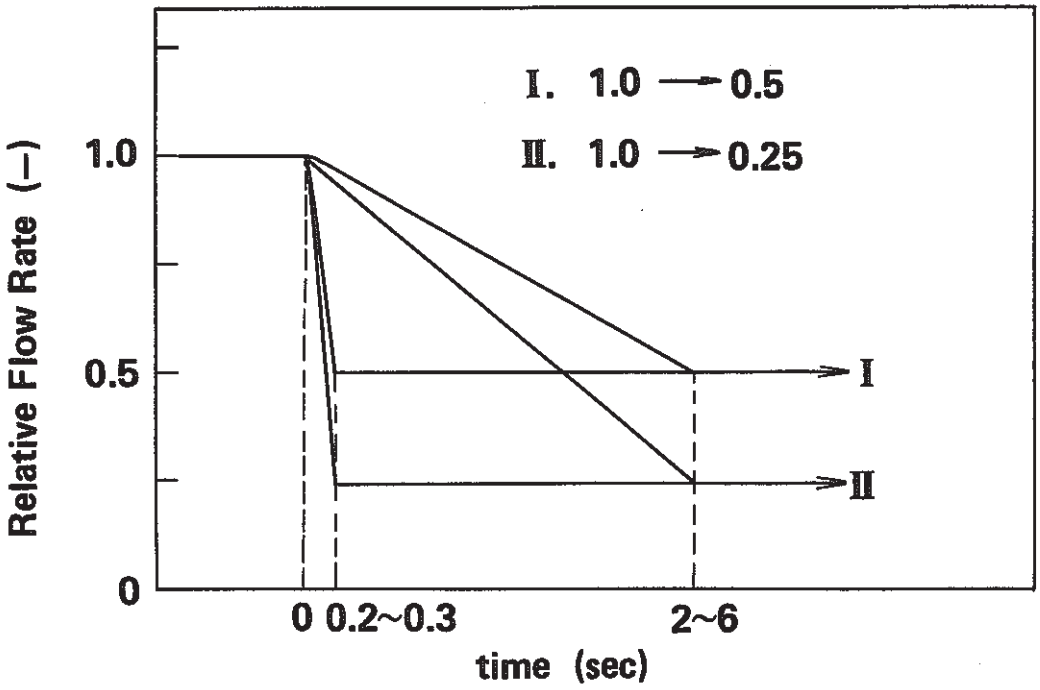

(a) Locus of Inlet Flow Rate in TRFD Experiment

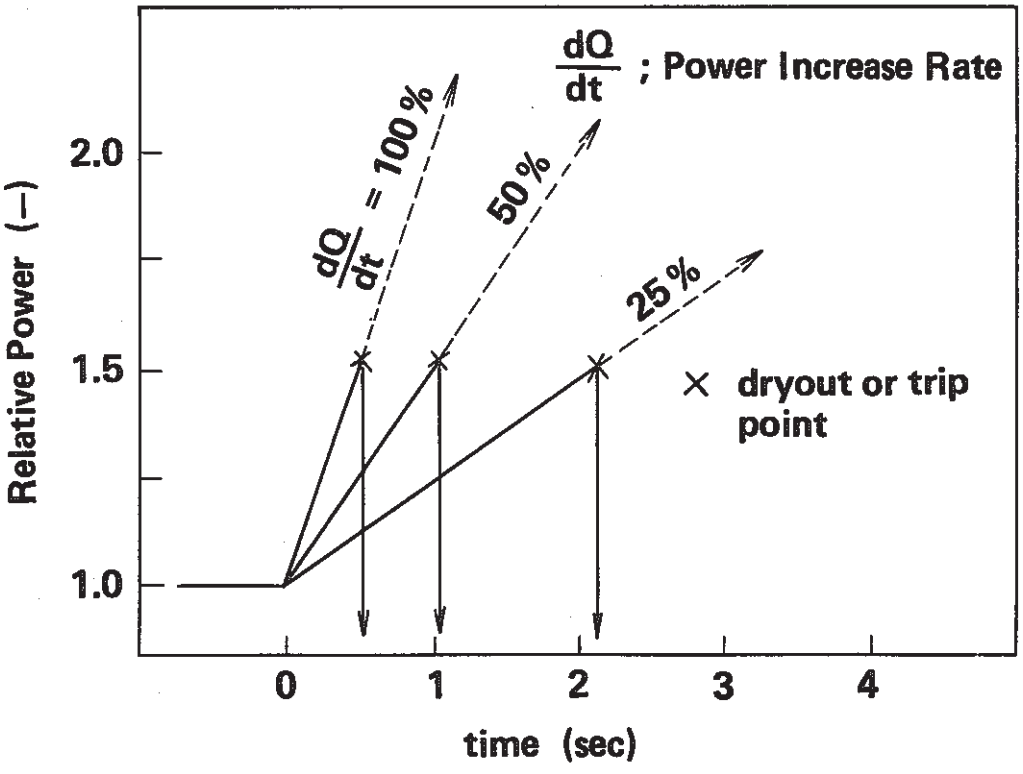

(b) Locus of Relative Power in TRPE Experiment

Fig. 3 Locus of Inlet Flow Rate and Relative Power in Experiment

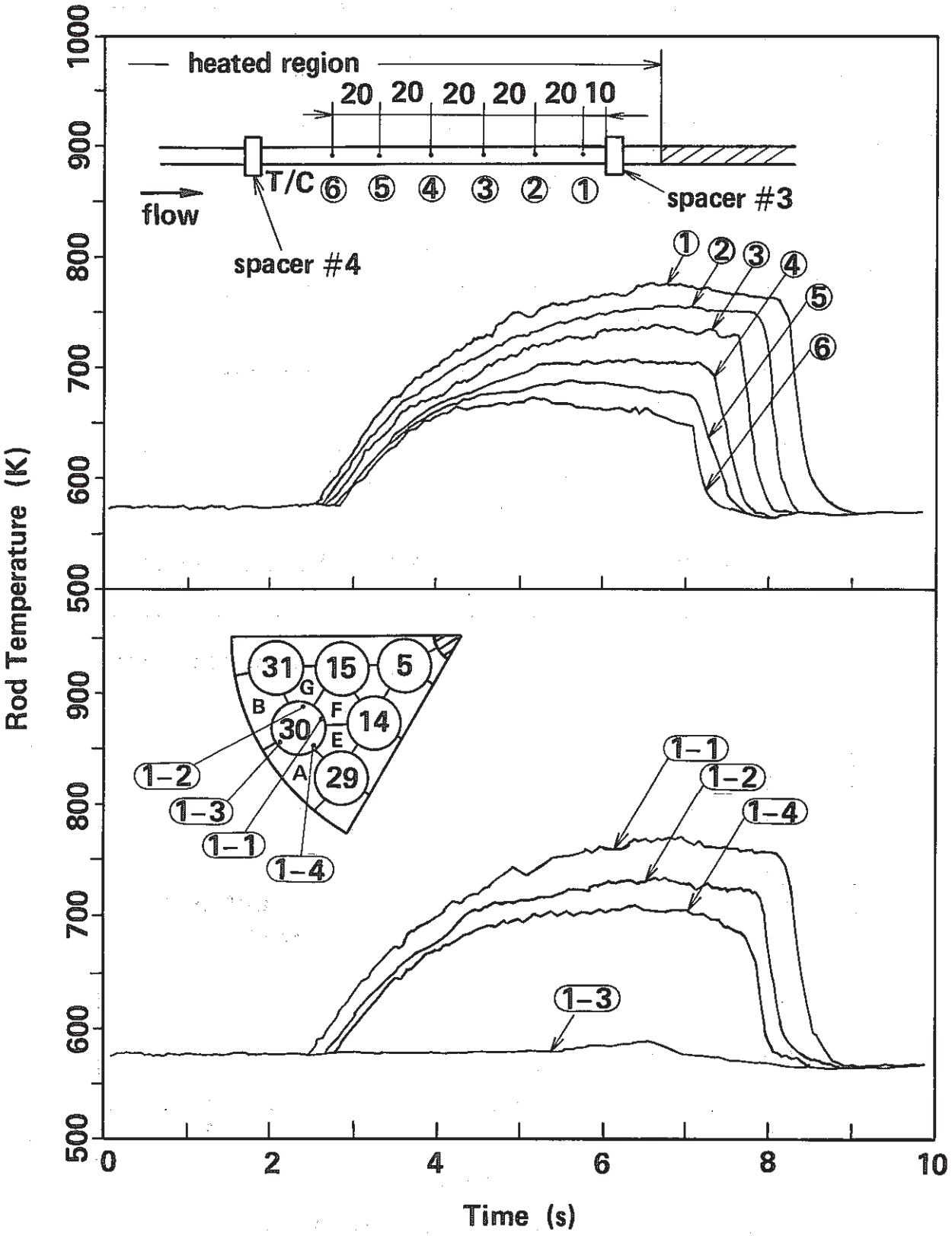

Fig. 4 An Example of Axial and Azimuthal Dryout Propagation and Temperature Distribution during Flow Transient (TRFD7006)

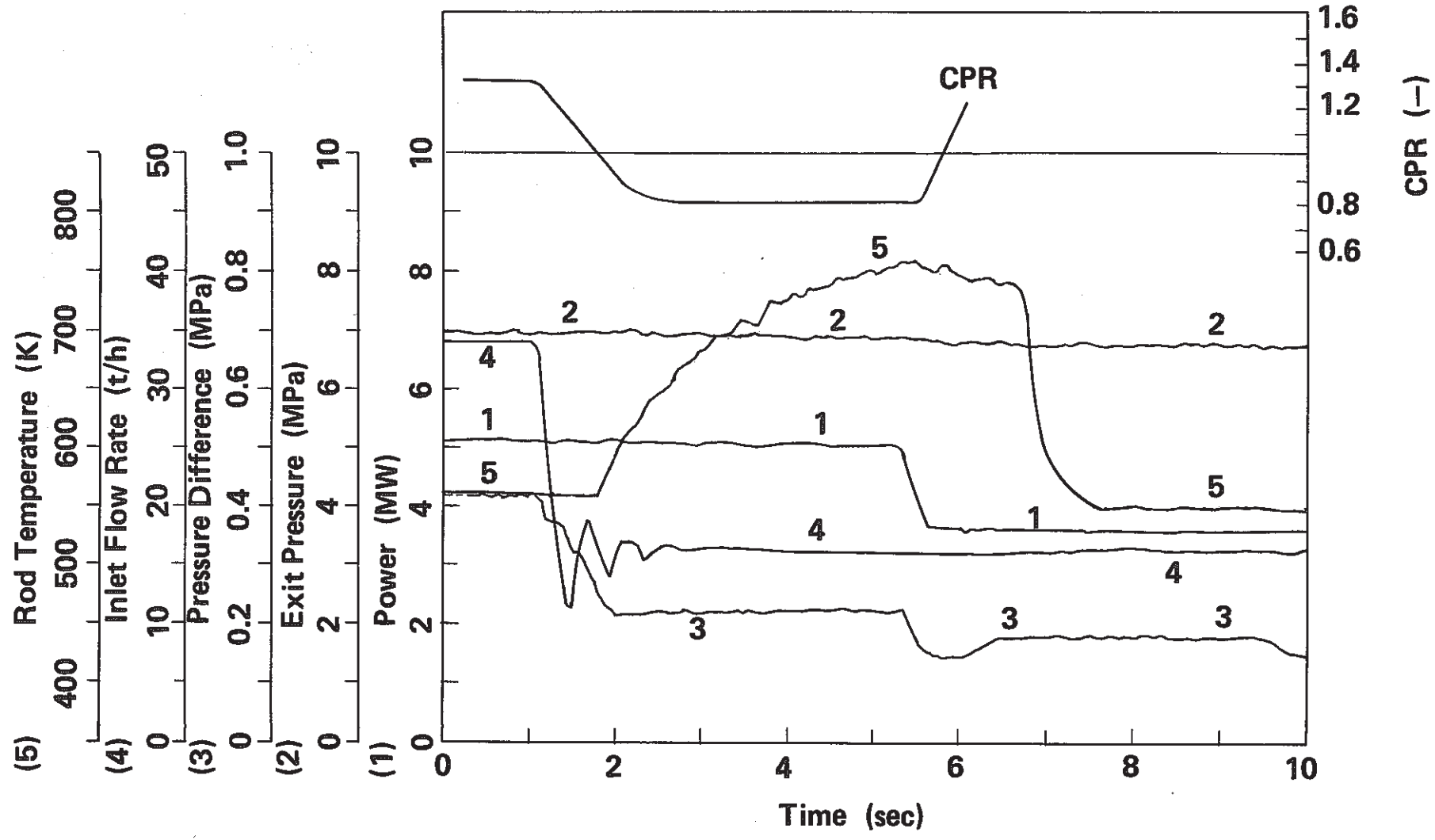

Fig. 5 An Experimental Result and Calculated CPR during Flow Transient (TRFD7006; P=7MPa, G_{ini}=2000kg/m^2·s, T_{in}=548K)

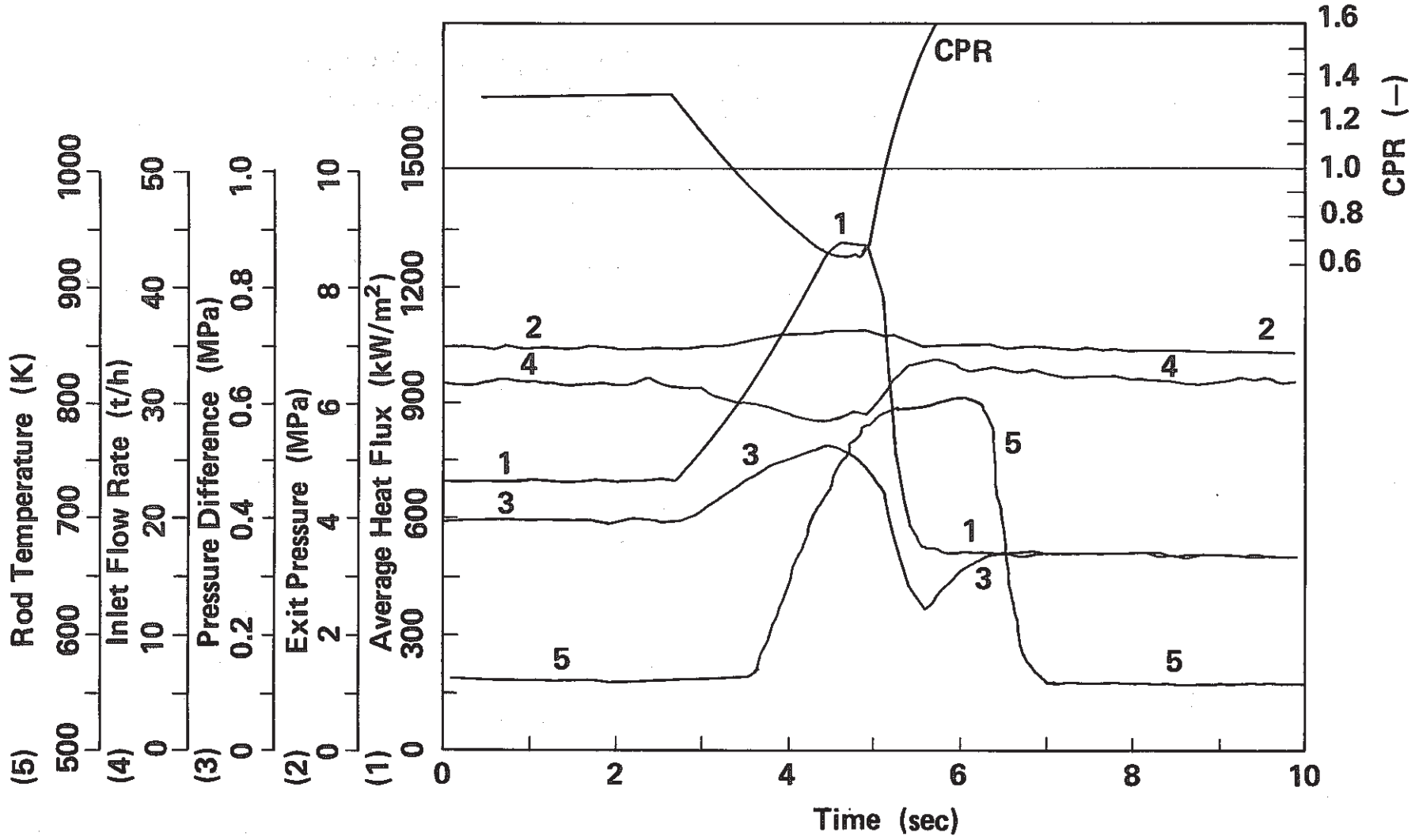

Fig. 6 An Experimental Result and Calculated CPR during Power Transient (TRPE7005; P=7MPa, G=1850kg/m²·s, T_{in}=548K, $\frac{dq}{dt}$=53%)

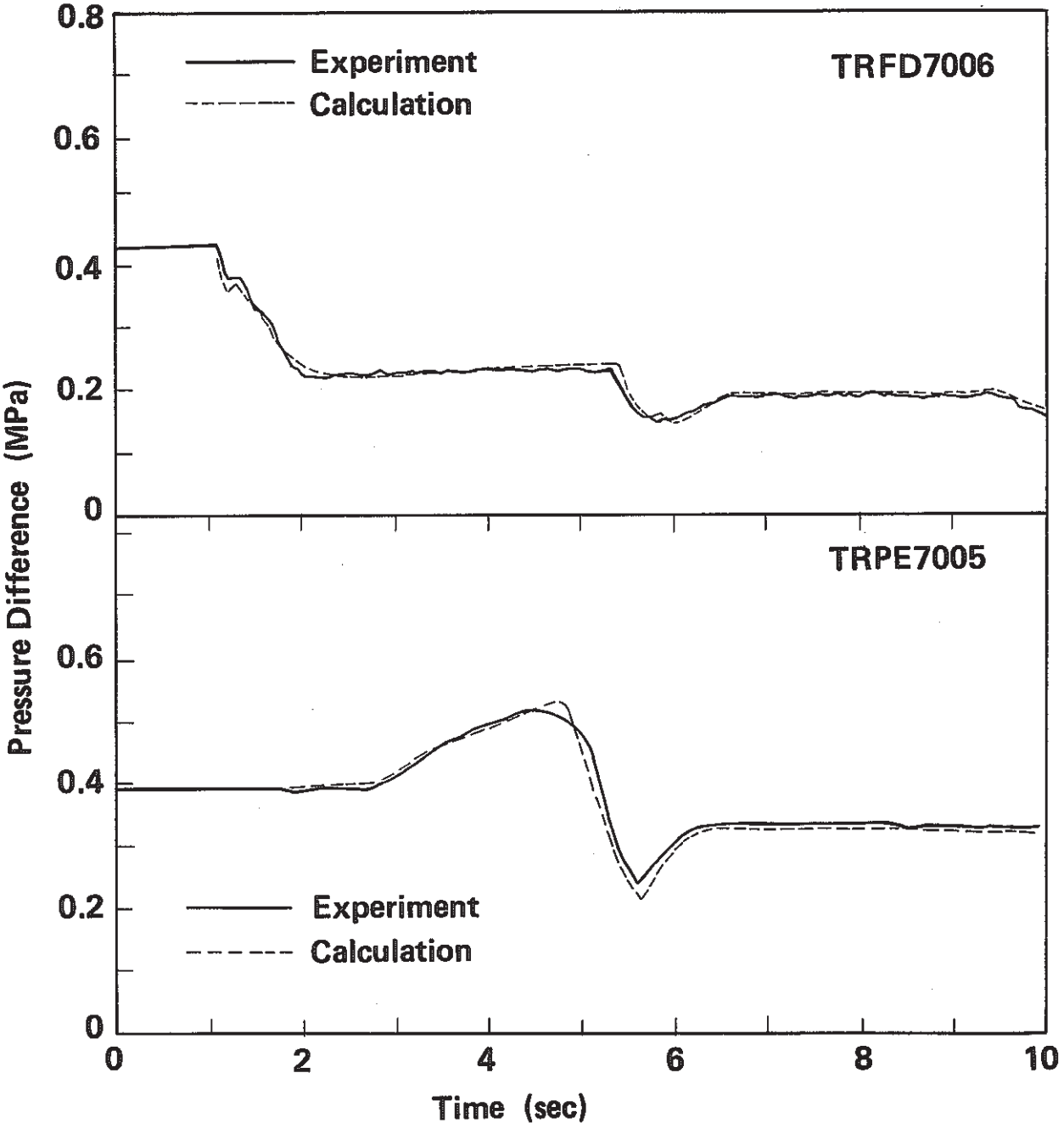

Fig. 7 Comparison between Calculation and Experiment on the Pressure Difference of Test Section Inlet and Outlet during Transients

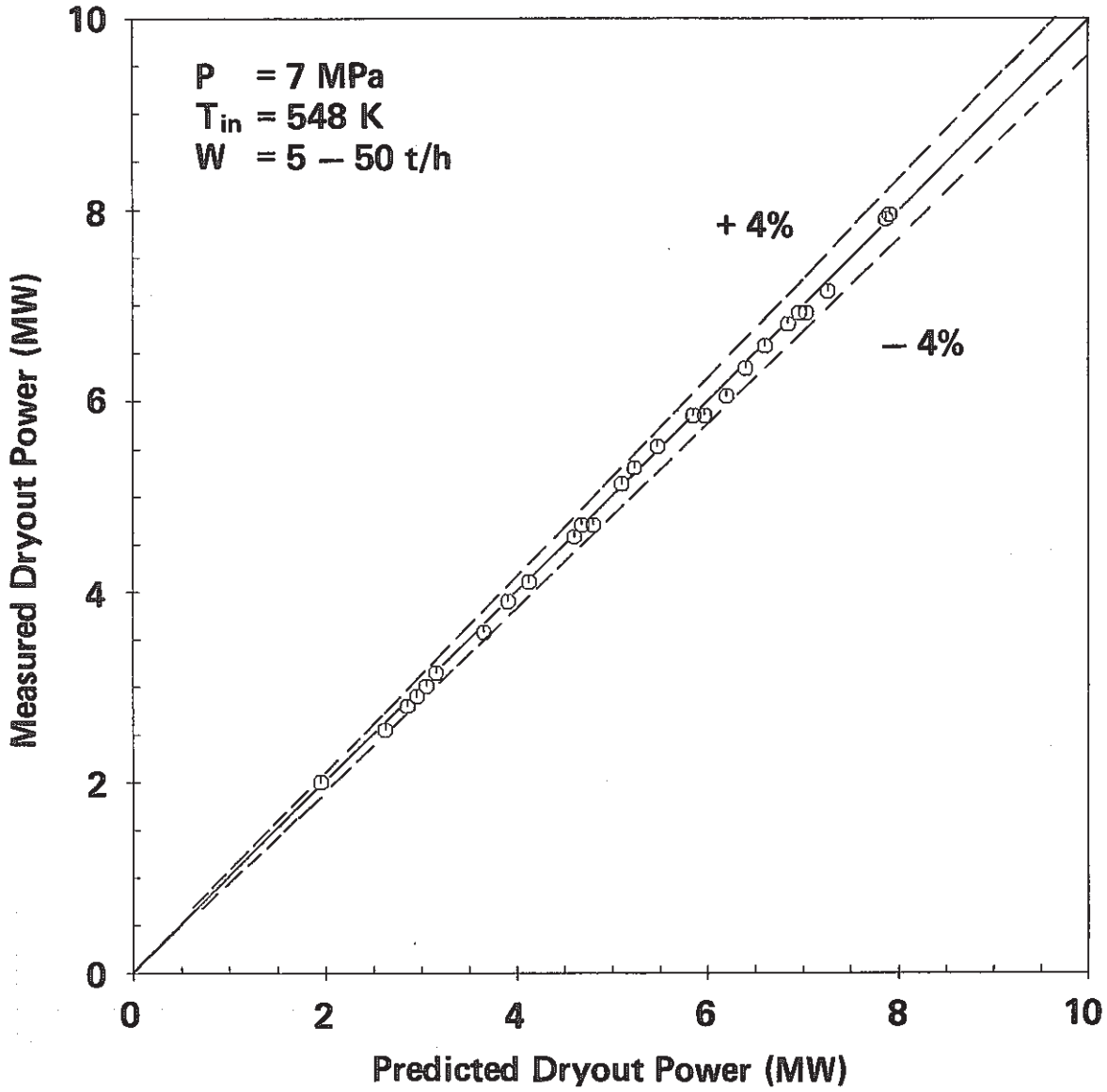

Fig. 8 Comparison of Steady State Dryout Power between Prediction and Measurement

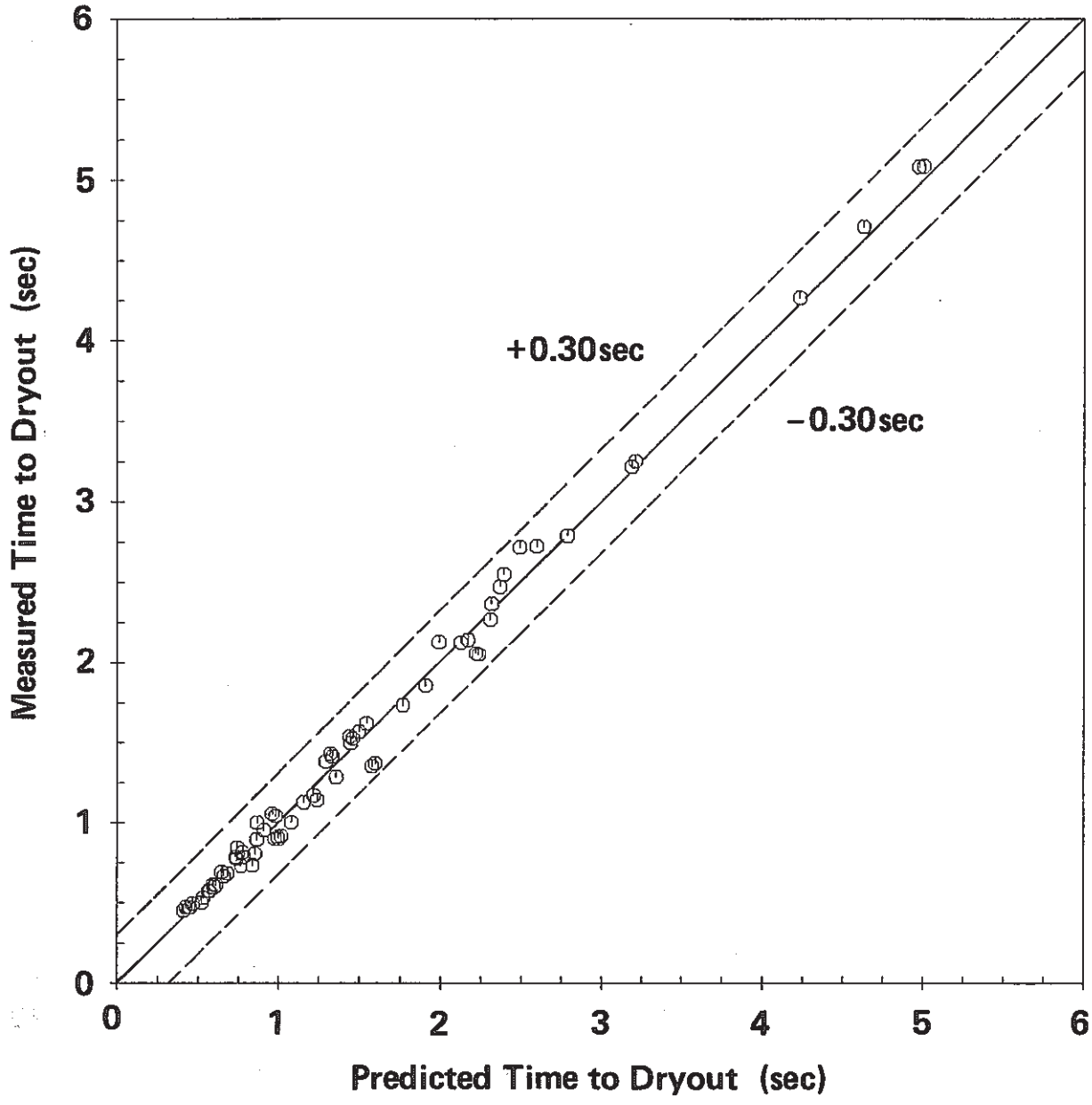

Fig. 9 Comparison between Predicted and Measured Time to Dryout during Flow Transient

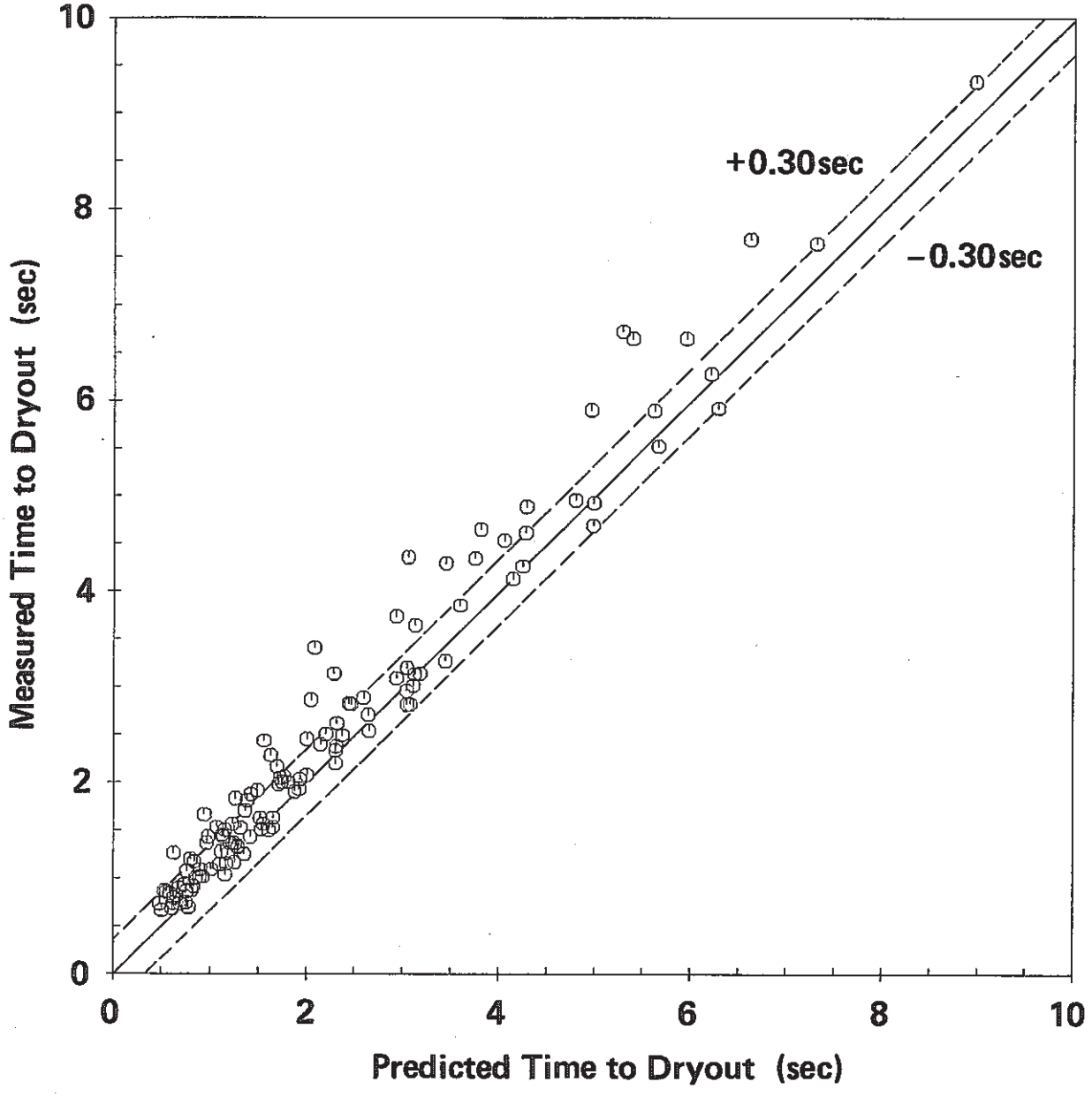

Fig. 10 Comparison between Predicted and Measured Time to Dryout during Power Transient

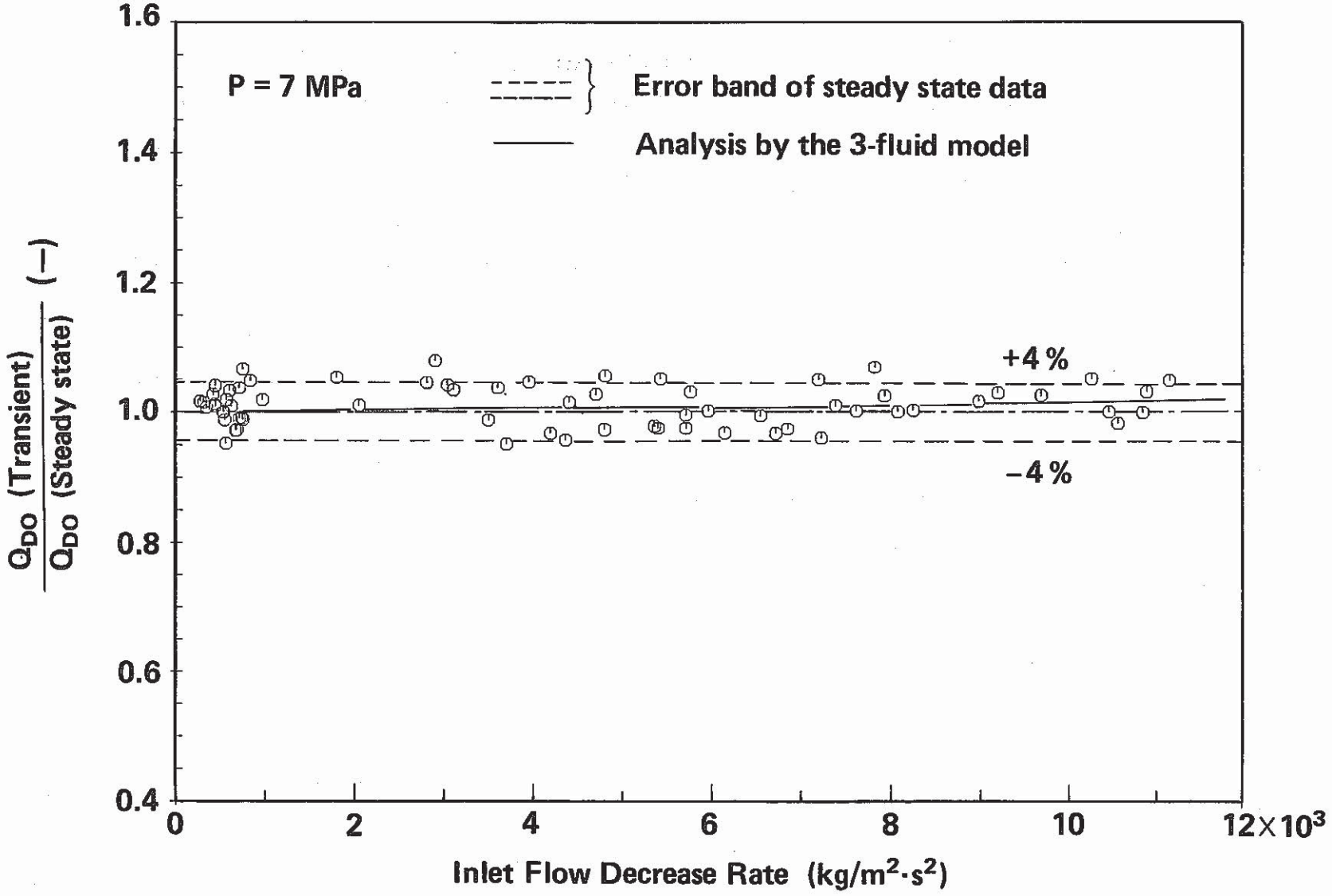

Fig. 11 Comparison between Analysis and Measurement on the Transient Dryout Power during Flow Transient

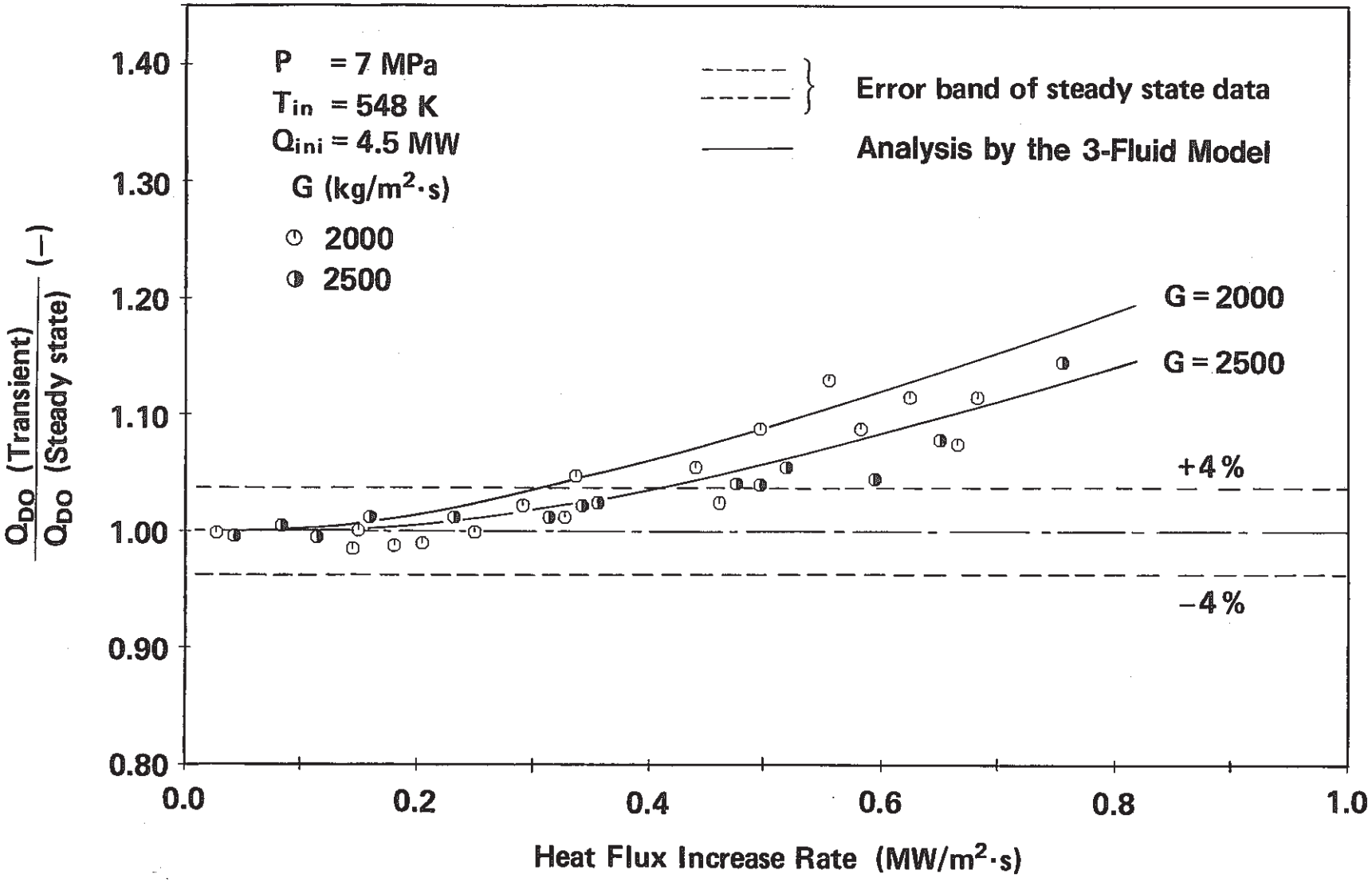

Fig. 12 Comparison between Analysis and Measurement on the Transient Dryout Power during Power Transient

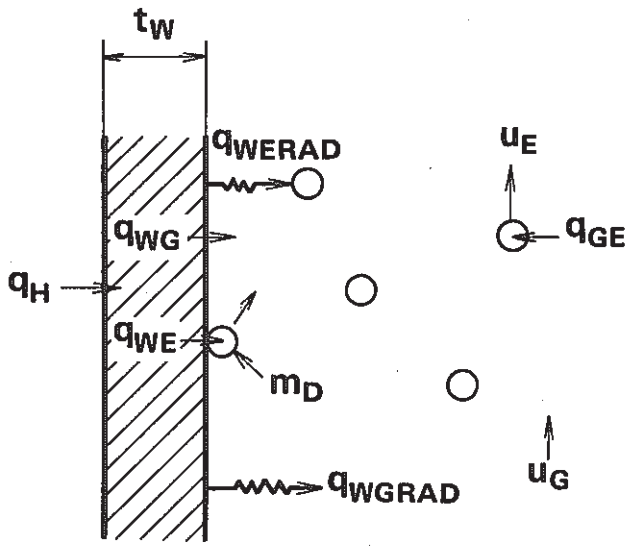

(a) Post-dryout Region

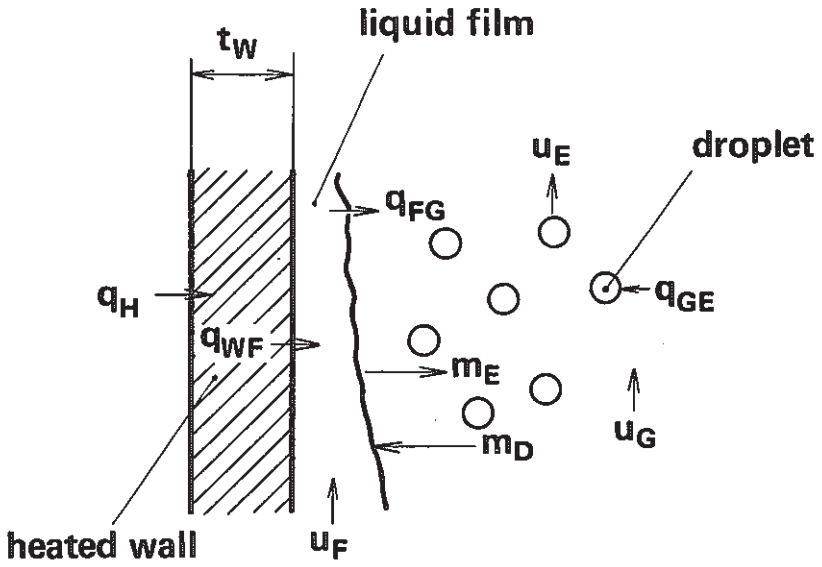

(b) Pre-dryout Region

Fig. 13 Three-fluid Heat Transfer Model